Rapid Prototyping J

Precise Determination of Initial Printable Time for Cement Mortar 3D Printing Using a Derivative Method

Journal:	*Rapid Prototyping Journal*
Manuscript ID	RPJ-03-2023-0087.R1
Manuscript Type:	Original Article
Keywords:	3D printing, Initial printable time, Initial width and height, Layer strain, Fiber reinforced mortar

Precise Determination of Initial Printable Time for Cement Mortar 3D Printing Using a Derivative Method

Abstract

Purpose: This study introduces a technique to accurately determine the initial printable time (t_{int}) and width/height of printed cement mortar. Precise t_{int} determination is essential for ensuring proper filament printing timing and eliminating the need for trial and error.

Methodology: The proposed technique establishes a mathematical relationship between width and time, using a derivative method to determine the t_{int} for each mortar. The study conducted experimental tests on t_{int}, layer strain, and the relationship between filament width and time. The tests involved plain mortar and mortar reinforced with micro-fiber at varying volume fractions. The t_{int} was determined analytically using derivative method.

Findings: Results show that the proposed technique accurately determines the t_{int}, as evidenced by the resemblance between expected and actual initial widths. FRM exhibits smaller t_{int} and displays smaller layer strains than plain mortar.

Originality: This study introduces a novel technique that utilizes a mathematical relationship to determine the t_{int} and height of cement mortar printing.

Keywords: 3D printing; Initial printable time; Initial width and height; Layer strain; Fiber reinforced mortar.

List of Abbreviations

t	Time (minutes)
w_t	Filament width at the corresponding time (mm)
t_{int}	Initial printable time (minutes)
w_{int}	Initial printed width or filament width printed at t_{int} (mm)
h_{int}	Initial printed height or filament height printed at t_{int} (mm)
h_n^{exn}	Accumulated expected height up to n layers of printed filament (mm)
h_n^{ac}	Accumulated actual height up to n layers of printed filament (mm)
ε_n	Layer strain or the ratio between the net deformation and the accumulated expected heights up to n layers

1. Introduction

The construction industry is known as a labor-intensive industry, especially in developing countries [1]. This can become a problem in countries with labor shortages and high labor costs. Low birth rates in some countries have led to an aging population, resulting in labor shortages, slow economic growth, and strain on government budgets. Since 2021, Thailand has been a fully aging society, with 20% of the population aged 60 years or older [2]. In 2020, the working-age population was 57 million, with 67% participating in the labor market. Over the past 7 years, the size of the labor force has shrunk by more than 1.2 million people [3], and the shortage is expected to increase by about 300,000 to 500,000 people in the coming year.

The introduction of advanced and automation technologies is expected to play a role in dealing with the upcoming worldwide labor shortage. For the construction industry, the current challenge in automation application can be broken down into three segments: automation of traditional physical tasks on-site (i.e., robots laying bricks or machines paving roads), automation of modular construction (i.e., precast or 3D printing of components), and automation and digitization in design, planning, and management procedures [4]. In the modular construction segment, 3D printing technology is currently a leading trend, but it is not a new technology, having been first developed in the 1980s. In the past decade, it has gained popularity, and the technology has significantly improved, making it more applicable for actual construction. The benefits of adapting 3D printing in construction include the reduction of costs related to labor and temporary structures, the increase in productivity related to construction time, the effectiveness in material usage, and the reduction of construction waste.

Regarding the use of cement material in 3D printing technology, the challenges are not only focused on the development of printing machines but also on the development of cement materials suitable for printing. Unlike conventional synthetic materials, the properties of cement materials change with time. At an early age, right after mixing, the cement is in liquid form, allowing it to flow freely in any direction. In this stage, cement is not able to be printed into a required form. However, as time passes, the plasticity decreases gradually along with the progressing hydration reaction between cement and water. Up to a specific time, called the 'initial printable time,' the properties of fresh cement become adequate for extrusion (or printing) and sufficiently stable to retain its shape after being printed. The 'final printable time' occurs when the cement begins to lose its ability to print properly or maintain the desired shape [5][6][7]. Therefore, the term 'workability' for cement printing mortar is relatively different from that of conventional cement mortar. The workability of cement printing mortar must satisfy three important properties: flowability, printability (or extrudability), and buildability.

The term printability refers to the ability of cement to be printed or extruded into a continuous and uniform filament with minimum or no defect. Since the fresh properties of cement change with time, the printability of cement mortar is strongly related to a specific time in which the cement mortar can and cannot be printed properly. The initial printable time refers to the time when a cement material can be extruded (or printed) continuously into a filament with uniform and stable dimensions and able to support its weight. On the contrary, the time when the cement cannot be printed continuously or in uniform dimensions is called the final printable time [8][9][10].

In general, there are several factors that affect the initial printable time of cement mortar, including cement content, pozzolan materials, and chemical admixtures, among others. Zhang et al. [11] conducted experiments on mortar with two different sand/cement (s/c) ratios (0.6 and 1.0) and found that the mortar with a higher s/c ratio exhibited a longer initial printable time. Regarding pozzolan materials, Zhang et al. [12] also investigated the effect of silica fume content and found a reduction in initial printable time with the addition of silica fume. Our previous study [9] also showed that the addition of a viscosity modifier agent (VMA) and microfiber led to a decrease in the initial printable time of cement mortar for 3D printing. Similar results were reported by Rubio et al. [13] on the effect of fiber, VMA, and silica fume on the initial printable time of cement mortar; the initial printable time decreased with the incorporation of either fiber, VMA, or silica fume into the mortar mix. Wu et al. [14] investigated the effect of recycled aggregates (RA) on cement mortar for 3D printing and found that the buildability of mortar increased with the increasing RA content.

In general, the initial printable time is considered a critical wet property that controls the printability of fresh mortar, allowing it to be printed continuously in a proper shape. Conventionally, the process of determining both initial and final printable times involves printing a series of mortar filaments in a specific time interval until the filament can be printed continuously without any defects and to the desired dimensions (either width or height). This method is simple and easy to perform, but the degree of accuracy depends strongly on the setup of the time interval. The accuracy increases as the time interval becomes smaller, but decreasing the time interval means that a larger number of tests must be performed, which could become uneconomical. Hence, the main objectives of this study is to introduce a new technique to accurately determine the initial printable time without having to print large numbers of cement mortar filaments. The proposed technique involves printing a number of mortar filaments at 5-minute time intervals and measuring the change in dimension with time. Then, the empirical relationship between dimension change versus time is determined, and a simple mathematical procedure is applied to determine the initial printable time. With the ability to accurately determine the initial print time, operators can begin the printing process without the need for trial and error, which leads to cost saving. This accuracy in timing also results in less deformation, allowing structures to maintain their shape and stability.

In addition to the time, the fresh cement mortar for 3D printing must possess a so-called "buildability" characteristic. The buildability includes the ability of fresh mortar to sustain loads from additional layers with minimum deformation or distortion [15][16]. Frequently, the failure of 3D printing structures comes from excessive deformations in the printed layers, which leads to geometry distortion and plastic collapse during printing. To prevent this, the layer deformation must be minimized [17][18], and this is the second objective of this work. In this study, micropolypropylene fibers were used to reduce the layer deformation of printed mortars. Fibers are known for their ability to improve both mechanical and physical properties of concrete, ranging from shrinkage reduction and durability enhancement [19][20], to impact resistance [21][22][23], toughness, and strength improvement [24][25]. Thus, the addition of microfiber into the mortar mix is expected to improve the buildability of printable mortar.

In summary, this study is motivated by the need for an accurate and efficient method to determine the initial printable time of fresh mortar in 3D printing. The conventional approach lacks precision and is economically impractical. Inaccurate determination of the initial printable time can lead to deformation and distortion in printed structures. The proposed methodology involves printing mortar filaments, analysing dimensional changes, and establishing an empirical relationship between dimension change and time. This eliminates the need for extensive filament testing and reduces reliance on trial and error. The structure of the paper consists of: 1) Introduction provides a literature review, problem statement, motivation, and proposes research method, 2) Experiment procedure section outlines the materials, equipment, mix proportions, and experimental methods, 3) Results and discussion, the findings pertaining to the initial printable time and layer strain are presented and analyzed, 4) Conclusion based on the obtained results and presents the limitations of the study and 5) References includes a list of all the sources cited in the research.

2. Experimental procedure

2.1. Materials

The binder phase comprised of Portland Cement type I (C) (ASTM C150) and silica fume (SF) with a particle size ranging from 0.03-0.30 µm and a specific surface area of 20,000 m^2/kg. The chemical composition of the silica fume is given in Table 1. River sand with a particle size that passed through sieve No.16 was used as the fine aggregate (FA). Micro polypropylene fiber (MF) with a length of 6 mm was used, and its properties are given in Table 2. Two types of chemical admixtures were used: superplasticizer type G (SP) (polycarboxylate type) was added to enhance the flow of mortar, while polyethylene glycol (PEG) was added as a water-retaining agent to prevent moisture loss during the printing process [26]-[28]. The chemical properties of PEG are given in Table 3.

Table 1 Chemical composition of silica fume (SF)

	SiO_2	Al_2O_3	Fe_2O_3	CaO	SO_3	LOI_{SF}
SF	88.30	1.17	4.76	0.48	1.05	-

Note: *Product Data Sheet (ELKEM MICROSILICA® 920), Elkem (Thailand) Co., Ltd., April 2023.*

Table 2 Properties of micro fiber (MF)

	Material	Length (mm)	Specific Gravity	Elastic Modulus (MPa)
MF	Polypropylene	6	0.91	3445

Note: *Product data sheet (Sika® Fibermesh®-150) Micro-synthetic monofilament fiber , Sika (Thailand) Co., Ltd. , November 2019*

Table 3 Properties of polyethylene glycol (PEG) [29]-[32]

Specification	Unit	Test result
Melting point	°C	42-46
Specific Gravity	at 25 °C	1.09
Flash point	°C	285
Heat of Fusion	Cal/g	37
Range of Avg. Molecular Weight		1305-1595
Physical Form		Flake

2.2. 3D printing machine

The printing machine used in this study was built and constructed at the Department of Civil Engineering, KMUTNB and was at a laboratory scale (Fig. 1). The machine had dimensions of 500x500 mm and consisted of a steel frame, mortar container, mortar injection system, nozzle, hose, and controlling unit. The specifications of the machine are given in Table 4.

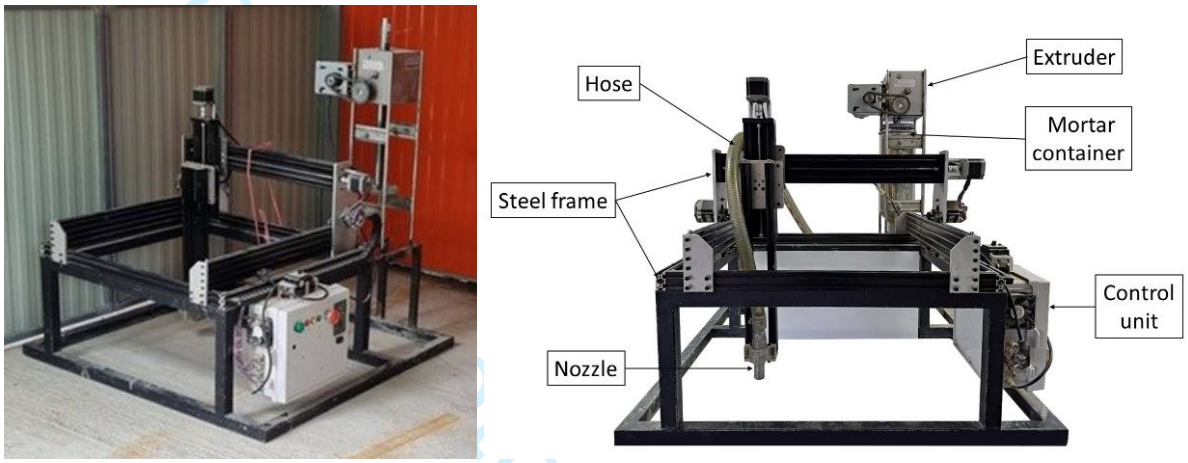

Fig. 1 3D Printing machine

Table 4 Printer specification

Properties		unit
Size	500x500	mm
Nozzle speed	≤2000	mm/minute
Container volume	4.5	litre
Nozzle dimension	10, 20	mm

2.3. Mix proportions

The mix proportion for a cubic meter of the control mix (M0) was set at 879 : 1171 : 213 : 88 : 24 : 97 kg (C: FA: Water: SF: PEG: SP). For fiber reinforced cement mortar, the MF was mixed with the control mix at the rate of 0.025% (MF25), 0.050% (MF50) and 0.10% (MF100) by volume. The mix proportions of all mortar types are shown in Table 5.

Table 5 Mix proportions of plain and fiber reinforced mortar

Mortar type	Material (per m^3)						
	C (kg)	FA (kg)	Water (kg)	SF (kg)	PEG (kg)	SP (kg)	MF (%V_f)
Control (M0)	879	1171	213	88	24	97	-
MF25							0.025
MF50							0.050
MF100							0.100

The mortar was prepared by dry mixing all solid components (except MF) in a mixer for about 1-2 minutes. The liquid part consisting of water, SF, and PEG was then added (note that this point in the process marks the start of the initial printable time test) and the mixing process continued for another

1-2 minutes. For fiber-reinforced mortar, the fibers were added last by evenly distributing them in the fresh mix, and the mixing continued for about 3 minutes. The fresh mix was then transferred to the container of the 3D printing machine, ready for the printing process.

2.4. Experimental series

The experimental series was designed to evaluate both the printability and buildability of mortar suitable for 3D printing applications. The initial and final printable times are two major components affecting the printability of the cement mortar. In the case of buildability, the main concerns are the ability of the printed mortar to resist the load from subsequent layers and to gain suitable mechanical properties in a short time. Thus, three experiments were carried out to investigate the desired properties: initial printable time, layer deformation, and layer strain. In addition, compressive, flexural strength, density, and water absorption tests were also performed on both cast and printed specimens.

2.4.1. Initial printable time test

Theoretically, the workability of fresh cement composite gradually decreases over time due to the hydration reaction. At the beginning, the high workability causes the width of the printed filament to be wider due to the outward flow. The width then decreases with time (or decreasing workability). After a specific time, a constant and uniform width is achieved, and this time is called the initial printable time.

This experiment employed this concept to evaluate the initial printable time of each mortar type. The test began by printing a filament of mortar with a length of 300 mm every 5 minutes on a glass plate, starting from the 25th minute until the printed filament came out continuously with a uniform dimension. After each filament was printed, the width was measured at three different locations (see Fig. 2), and the average of the three locations was used as representative data for that mortar printing in that time. The same process was repeated every 5 minutes until the last filament was printed (at the 70th minute). Using the obtained data, the relationship curve between width (w_t) and time (t) can be plotted, as shown in Fig. 3. Using the plotted curve, an empirical equation related to the change of width over time can be determined (Eq.1).

$$w_t = f(t) \quad (1)$$

Where t is time (minutes), w_t is the width at the corresponding time (mm).

By setting the derivative of Eq.1 to zero, the time when the width became narrowest and remained constant was obtained (Eq.2). This time was set as the initial printable time (t_{int}) of the tested mortar, i.e., when the constant width of the printed filament was achieved.

$$\frac{dw_t}{dt} = 0 \rightarrow t = t_{int} \quad (2)$$

The same procedure was repeated for all concrete types to obtain the corresponding t_{int}.

By substituting t_{int} back into Eq.1, an initial width (w_{int}), where a printed filament becomes stable and achieves a constant width without defect, can be determined.

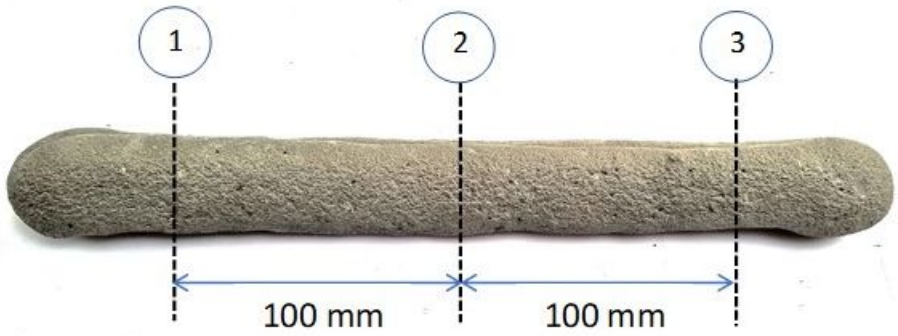

Fig. 2 Width measurement location

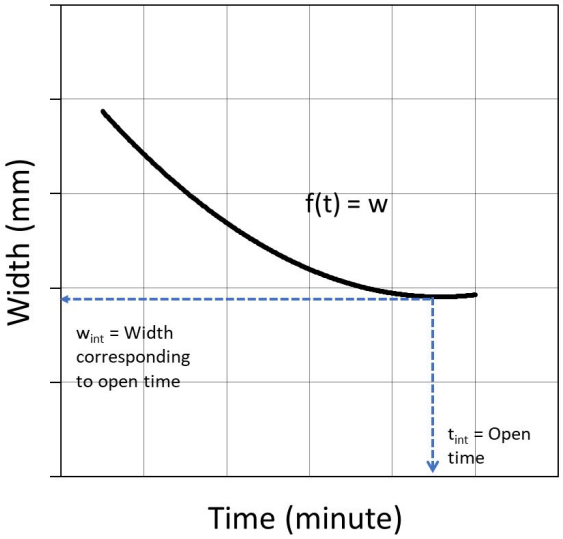

Fig. 3 Illustration of the ideal curve for width vs time

2.4.2. Layer strain test

Layer deformation or layer strain test is an experiment used to measure buildability or the ability of the fresh mix to support loads from additional printed layers. The layer deformation can be measured directly from the height of the layer being printed [33][34] and used to determine the layer strain [35].

The experiment began with the determination of both initial and accumulated expected printed heights. To obtain the initial printed height, a filament for each type of mortar was printed at the initial printable time obtained from 2.4.1. After printing, the height was measured from three different locations, and the average value was used as the initial printed height (h_{int}).

The h_{int} was used to calculate the accumulated expected height based on the number of layers being printed (Eq.3).

$$h_n^{exp} = n.h_{int} \quad (3)$$

Where n is the number of printed layers.

The layer deformation test began by setting up a nozzle with a clearing height of 15 mm. The first layer of each mortar type was printed at the time t_{int} corresponding to the mortar type. The height was measured at three different locations (Fig.2), and the average value was used to represent the initial printed height (h_{int}) of a filament. After finishing the measurements, a subsequent layer was printed

on top of the existing mortar filament with a 5-minute time gap (Fig. 4a). For each additional layer added to the mortar filament, the accumulated actual printed heights corresponding to the number of printed layers (h_2^{ac}, h_3^{ac}…h_n^{ac}) were measured, averaged, and recorded (Fig. 4b and 4c). Up to 5 layers were printed for each type of mortar.

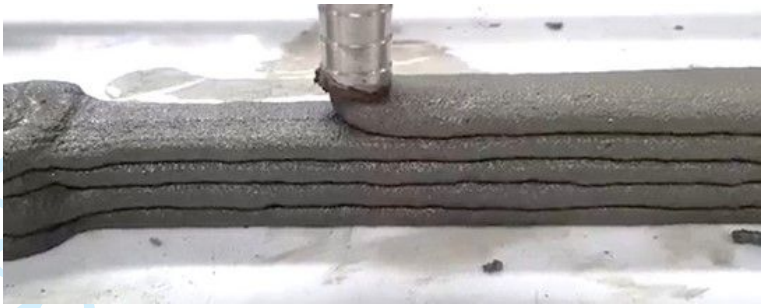

(a)

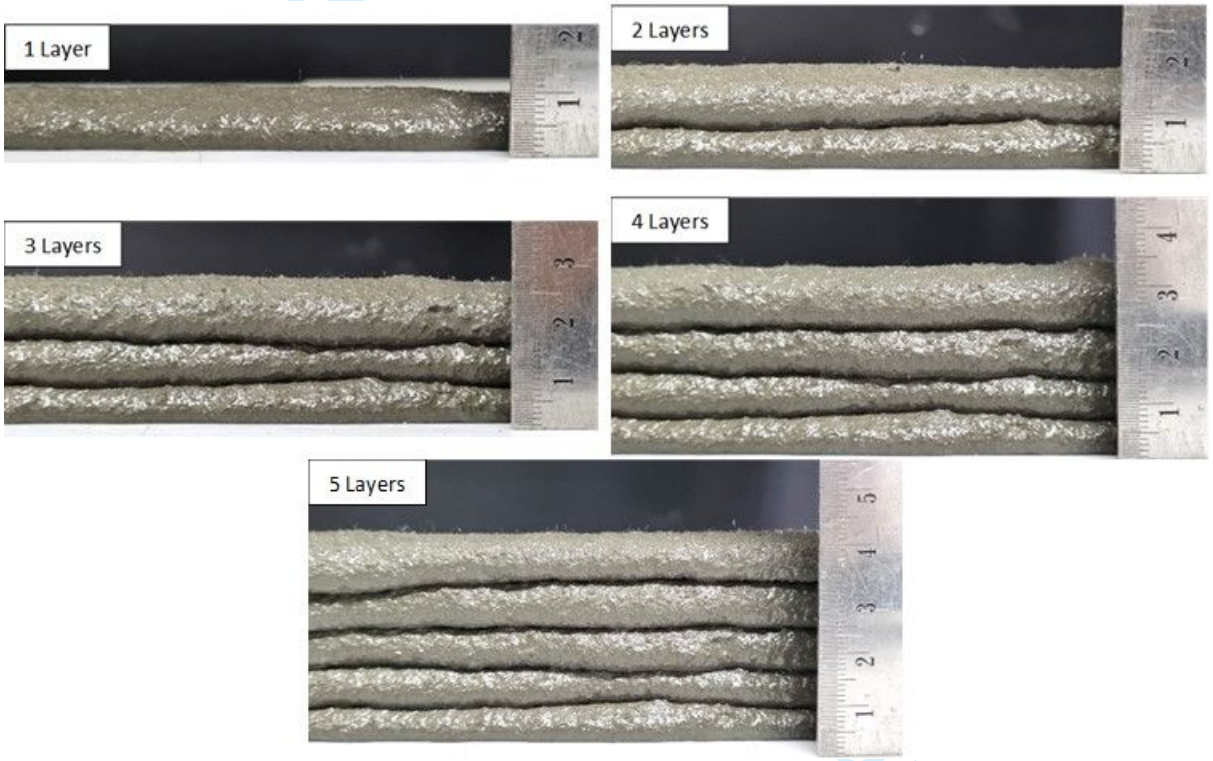

(b)

(c)

Fig. 4 Layer strain test process: (a) Printing process, (b) manual measurement of layer heights, and (c) recording of accumulated actual height measurements

Using both results, the layer strain (ε_n) or the ratio between the net deformation (or the difference between expected and actual height up to *n* layers, Δh_n) and the accumulated expected heights up to *n* layers can be calculated using Eq.4.

$$\varepsilon_n = \frac{\Delta h_n}{h_n^{ex}} = \frac{(h_n^{ex} - h_n^{ac})}{h_n^{ex}} \quad (4)$$

3. Results and discussion

3.1. Initial printable time

As mentioned earlier, the initial printable time (t_{int}) refers to the time when a mortar filament begins to stabilize and remain at a constant width without defect after being printed. The test began by printing a series of cement mortar filaments every 5 minutes. The width of each filament was measured at several locations along the length, and the average was determined. Results on the relationship between width versus time are plotted in Fig. 5.

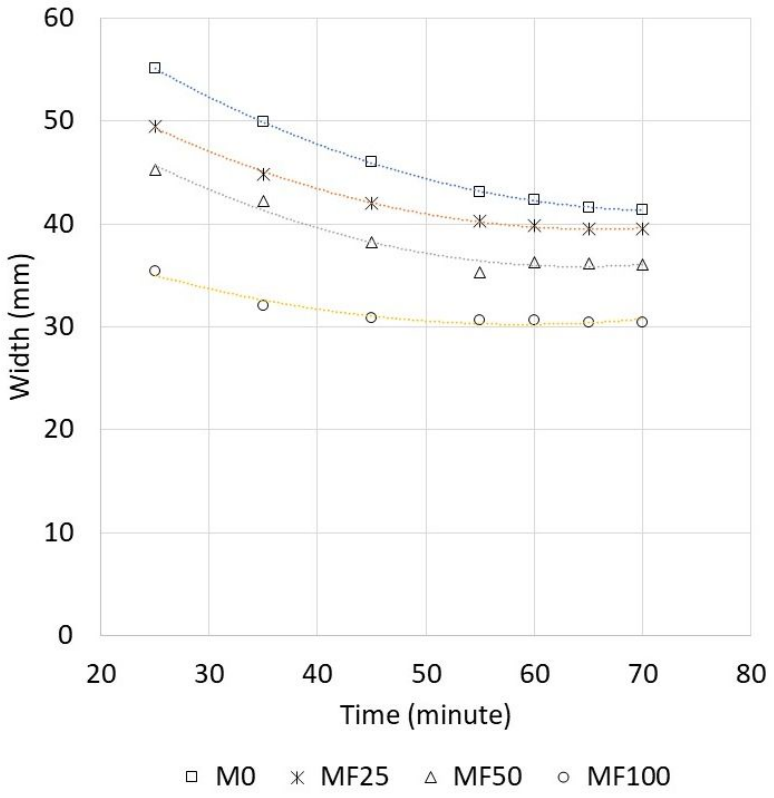

Fig.5 Relationship between width vs time of printed mortar

Fig. 5 shows the relationship between width and time of printed mortar for all mortar types, regardless of fiber content. The typical relationship indicated the change of width with respect to time, i.e., decreasing. At the beginning of the printing process, all mortar types exhibited larger widths. With passing time, the width gradually became narrower, and after a certain time, a constant width was

achieved (Fig. 6). Chen et al. [37] also reported that the average width of the cement filament tended to decrease with initial printable time due to the hydration of cement with time. Thus, determining the operation window is important to avoid nozzle blockage and disruption.

Fig. 6 Change of mortar width vs. time of plain mortar

The width change is primarily due to the hydration reactions of cement, which causes the mortar to become stiffer with increasing age [36][37]. At the early stage, the workability of fresh mortar was still high, which made it flow outward freely after being printed. As time passed, the fluidity decreased, and the mortar became stiffer. Though this decreased the flowability of the mortar, it helped lower the outward flow and increased the dimension stability.

For plain mortar (M0), a width of about 55 mm was observed at the 25th minute. As time passed, the width decreased, and the narrowest width of around 42 mm was observed at around the 70th minute. In the case of MF mortar, the 25th minute widths of all MF types were smaller than that of M0. This is due to the effect of the microfibers, which provided support to the fresh mix immediately after being printed. The 25th minute widths of MF25, MF50, and MF100 were observed as about 49.5, 45.3, and 35.4 mm, respectively. Similar to plain mortar, the width of MF mortars also decreased with time, which was solely due to the process of cement hydration reaction with time. In addition, comparing the specimens at the same printing time, the width of mortar was found to decrease with increasing fiber content. This was due to the effect of the fiber providing support and increasing water requirement, which caused the fresh mortar to become stiffer, with less outward flow and more dimensional stability. A comparable report by Chen et al. [38] on the effect of polypropylene and polyvinyl alcohol fiber on 3D printed cement composites also found a decrease in structure deformation with increasing fiber content due to the interlocking of the fibers.

The narrowest width of all the MF mortars fell in the range of 30 to 40 mm between the 60th to 70th minute. The initial width (width corresponding to time t0) can be determined after the initial printable time is calculated.

Using the results plotted in Fig. 5, the relationship between time and width can be drawn as shown in Eq. 8-11.

M0 $$w_t = 0.0061t^2 - 0.8845t + 73.404 \quad (8)$$

MF25 $$w_t = 0.0059t^2 - 0.7780t + 65.098 \quad (9)$$

MF50 $w_t = 0.0064t^2 - 0.8205t + 62.244$ (10)

MF100 $w_t = 0.0042t^2 - 0.4912t + 44.713$ (11)

By setting the derivative of Eq. 8-11 to zero (Eq. 2), the initial printable time (t_{int}) corresponding to each mortar type can be determined as shown in Table 6. The initial printable time of M0 was observed at around 72.5 minutes. The incorporation of fibers into the mortar mix caused the initial printable time to decrease gradually with increasing fiber content. The reason could be because of the increased specific surface area from adding fibers, which reduced the water availability, created a drier fresh mix, and lowered the initial printable time.

By back substituting t_{int} into Eq.8-11, the expected initial width (w_{int}) can be obtained (Table 6). The w_{int} of plain mortar was calculated to equal 41.3 mm, which was the highest among the specimens. The w_{int} decreased with the addition of fiber to the fresh mix. Comparing between the MF specimens, the w_{int} decreased gradually with the increasing fiber volume fraction. The smallest w_{int} of 30.4 mm was obtained in MF100 where the fiber content was the highest (0.10% volume fraction). The decrease in w_{int} was a direct result of the microfibers providing immediate support to the fresh mix which allowed the mortar to maintain its height better than the non-fiber mix [9].

Table 6 Initial printable time and initial width of cement mortar

Mortar type	t_{int} (minute)	Expected w_{int} (mm)	Actual w_{int} (mm)
M0	72.5	41.3	41.6
MF25	67.1	38.5	39.0
MF50	64.1	35.9	36.2
MF100	58.5	30.4	30.7

The comparison between the expected initial width (calculated using the derived t_{int} in equations 8-11) and the actual initial width (measured from the narrowest printed filament) reveals a close similarity, with the actual widths slightly larger than the expected widths by only approximately 0.6 to 1.2%. This resemblance between the two values suggests that the initial printable time obtained through the proposed method is highly accurate and can be effectively utilized to predict the initial printed width.

3.2. Layer strain

By printing each mortar using t_{int} obtained from 3.1, the initial printed height (h_{int}) of each mortar type was obtained. Also, by substituting h_{int} into Eq.3, the accumulated expected height up to 5 layers (h_5^{ex}) can be determined, as shown in Table 7.

According to the test results, the smallest h_{int} of 8.5 mm was observed in plain mortar, M0. The height then increased gradually with increasing fiber content. The MF100, which had the highest fiber content of 0.10%, exhibited the largest h_1^{ex} of 10.1 mm. This increase in height was due to the ability of the fibers to support the fresh mortar which allowed the mortar to maintain a vertical shape (with less outward flow) better than plain mortar.

It was also noticed that the height was inversely proportional to the width of the print mortar filament. Since the volume of mortar being extruded from the nozzle was the same for all mortar types, the mortar with larger width will exhibit lower height. For M0, as there was no support from fibers, the

print filament tended to flow outward horizontally more than that of MF mortar, causing the height to be lower.

Table 7 Initial (1st layer) height and accumulated expected height up to 5 layers

Mortar type	h_{int} (mm)	h_5^{ex} (mm)
M0	8.5	42.3
MF25	9.0	44.9
MF50	9.4	47.1
MF100	10.1	50.6

The test results for the accumulated actual vs expected heights are shown in Fig. 7. When additional loads (from additional layers) were added to the print filament, settlements were observed which caused the accumulated actual height to be smaller than the accumulated expected height. For example, the accumulated actual vs expected height at 5 layers (h_5^{ac}/h_5^{ex}) for M0, MF25, MF50, and MF100 was observed at 30.9/42.3, 34.2/44.9, 37.7/47.1, and 41.8/50.6 mm, respectively. The larger h_5^{ac} of MF compared to M0 indicated the support provided by the fibers.

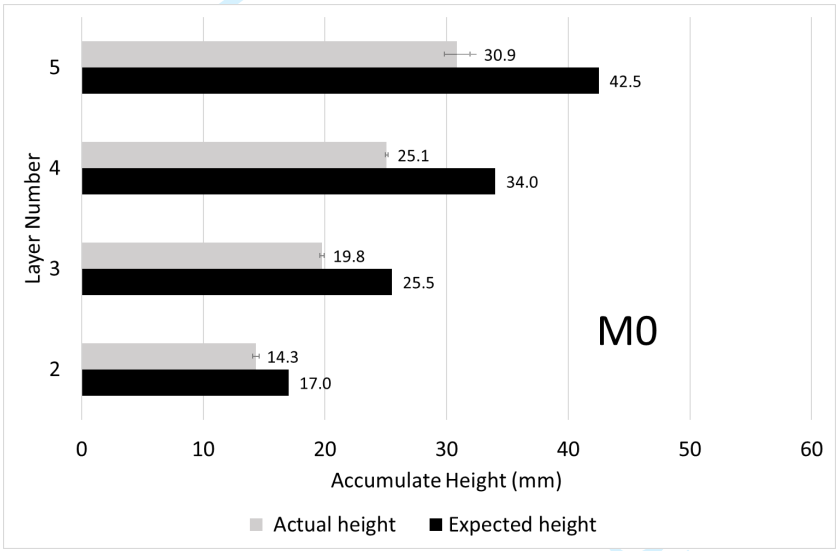

(a)

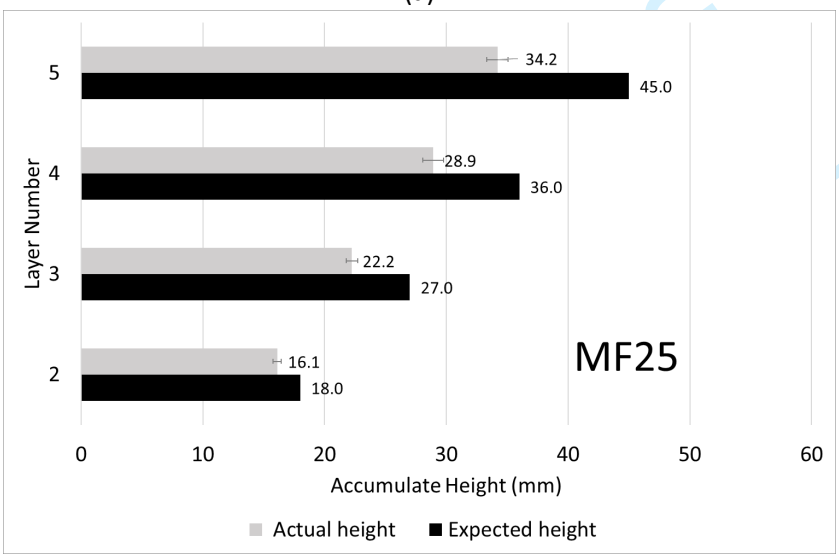

(b)

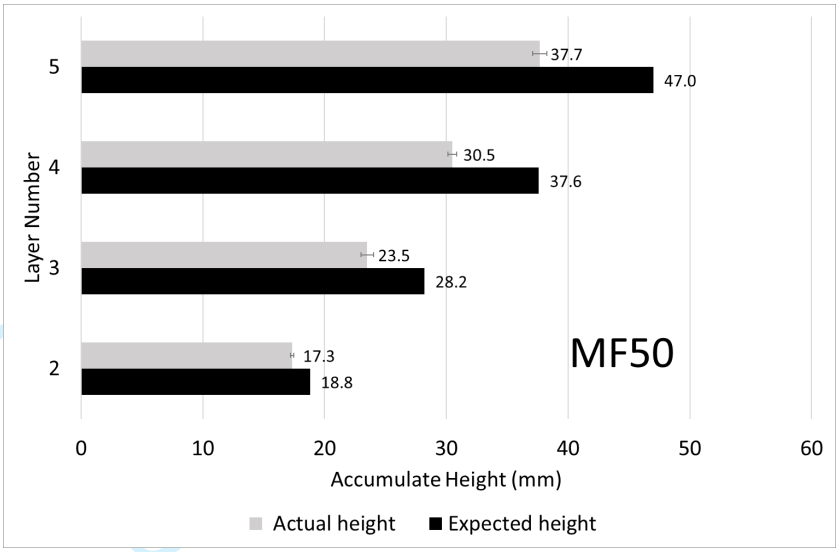

(c)

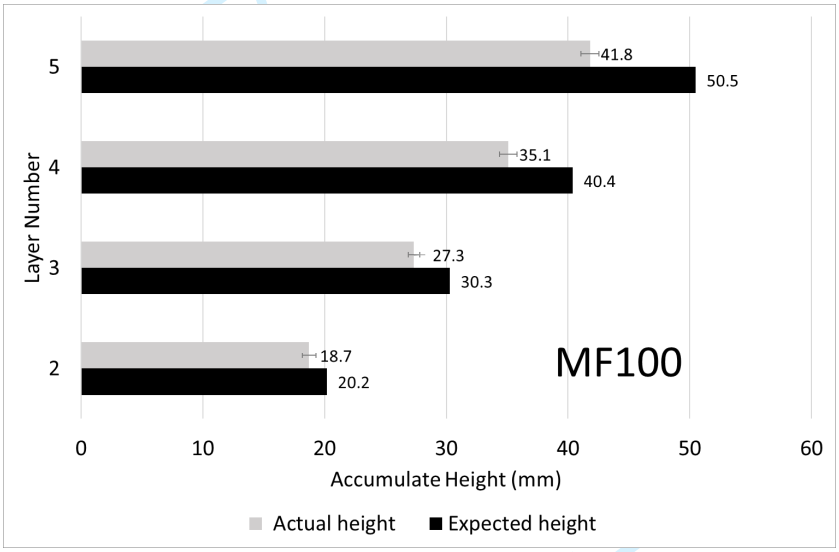

(d)

Fig. 7 Accumulated actual vs expected height of (a) M0, (b) MF25, (c) MF50 and (d) MF100

To generalize the comparison, the layer strain was calculated using Eq.5 and the results are shown in Fig. 8. With an additional layer of mortar filament printed on, the layer deformation occurred in the sublayers which led to the deformation of the overall structure. The layer strain of M0 was found to be the highest among the specimens with a layer strain of 0.16, 0.22, 0.26, and 0.27 for ε_2, ε_3, ε_4, and ε_5, respectively.

In the case of MF, the layer strain was lower than M0 for all fiber contents. The layer strain also decreased gradually with increasing fiber content. The lowest layer strain of 0.07, 0.10, 0.13, and 0.17 was observed in MF100 for ε_2, ε_3, ε_4, and ε_5, respectively. This is because of fibers providing support to the fresh mix, and when fiber content was increased, a larger number of fibers participated in supporting the printed layer which led to the decrease in layer deformation of the overall structure.

In terms of the number of layers, the data clearly demonstrates that as the number of layers increases, the layer strain consistently shows an upward trend for each mortar type. For M0 mortar, the layer strain increased by approximately 15.7% from 1 to 2 layers, followed by a substantial increase of 43.3%

from 2 to 3 layers. The subsequent addition of each layer resulted in smaller increases of approximately 16.5% (3 to 4 layers) and 4.2% (4 to 5 layers). Similarly, in MF25 mortar, the layer strain increased by approximately 10.6% (1 to 2 layers), 18.7% (2 to 3 layers), 9.6% (3 to 4 layers), and 22.5% (4 to 5 layers). For MF50 mortar, the layer strain showed increases of approximately 7.8% (1 to 2 layers), 14.7% (2 to 3 layers), 13.2% (3 to 4 layers), and a slight increase of 5% (4 to 5 layers). Lastly, in MF100 mortar, the layer strain increased by approximately 7.3% (1 to 2 layers), 3.6% (2 to 3 layers), 33.7% (3 to 4 layers), and 31.3% (4 to 5 layers). These findings highlight that an increase in the number of layers during the printing process leads to a gradual but varying increase in layer strain across different mortar types. This accumulation of layers has the potential to influence the structural integrity and properties of the printed mortar filaments.

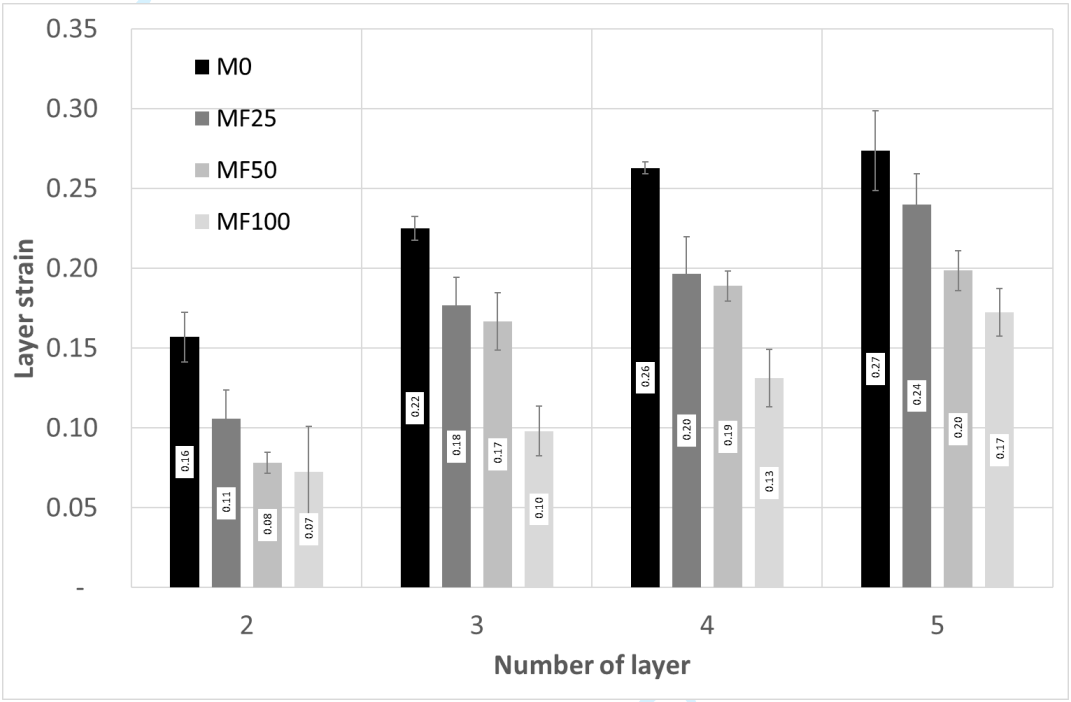

Fig. 8 Layer strain vs Number of layers

3.3. Microstructure and EDS analysis

3.3.1. Raw materials

In this section, the microstructures of raw materials used in this study are examined using a Scanning Electron Microscope (SEM). The raw materials include cement, silica fume, and micro-polypropylene fiber. Microscopic images and the results of Energy-Dispersive X-ray Spectroscopy (EDS) analysis were obtained and illustrated in Fig. 9 and 10, respectively.

The SEM image of cement reveals angular-shaped cement particles, a result of the grinding process during manufacturing (Fig. 9a). This grinding action helps in achieving the desired fineness of the cement particles, ensuring proper reactivity and performance in concrete applications. The presence of particles with a spiky shape in the SEM image indicates that they have undergone pre-hydration due to the presence of moisture. Pre-hydration can occur when cement particles are exposed to water or high humidity conditions during storage before their intended use.

In contrast to the angular cement particles, the SEM image also reveals the round-shaped particles of silica fume (as shown in Fig. 9b). Silica fume is a highly reactive pozzolanic material commonly used as

a supplementary cementitious material. Despite its round shape, which typically suggests good workability, the high specific surface area of silica fume, resulting from its extremely small particle size, can actually pose challenges to the workability of fresh concrete when added as an admixture.

Additionally, the SEM analysis also provides insights into the fiber reinforcement within the concrete matrix. The fibers, as seen in Fig. 9c, exhibit a smooth surface and possess a circular cross-section. It's worth noting that the imperfect appearance of both fiber ends is a result of the cutting process during manufacturing, which is a typical occurrence and does not significantly impact their performance within the concrete matrix.

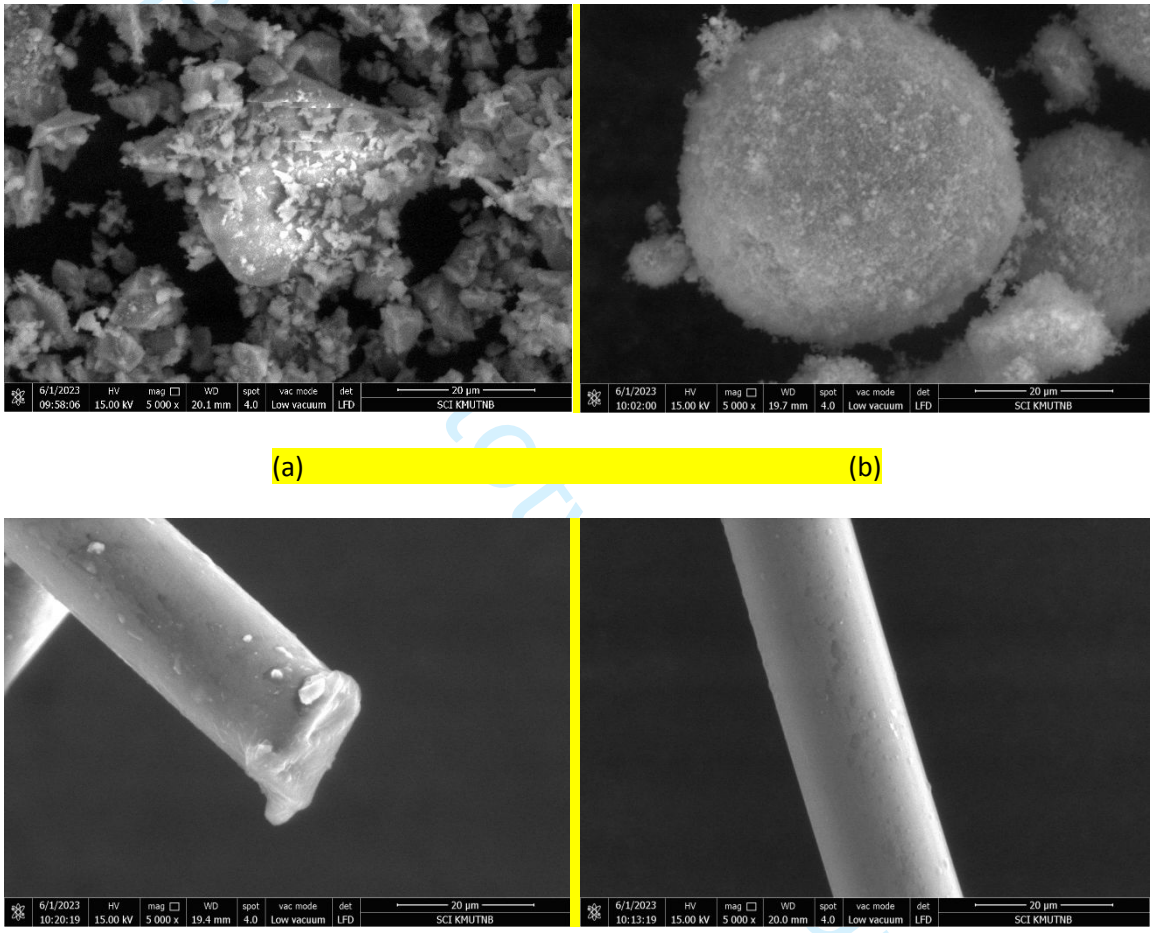

(a) (b)

(c)

Fig. 9 SEM images of raw materials: (a) Portland cement, (b) Silica fume, and (c) Fiber at 5000x

The EDS analysis of cement indicates that cement primarily consists of calcium (Ca) and oxygen (O) (Fig. 10a). These findings align with the known characteristics of cement, which is primarily composed of calcium silicates ($CaSiO_3$ and Ca_3SiO_5) as its main constituents. The high calcium content observed in the EDS analysis confirms the presence of calcium compounds in cement, such as calcium silicates, calcium hydroxide ($Ca(OH)_2$), and calcium carbonate ($CaCO_3$). These compounds play a crucial role in the hydration process of cement, contributing to the development of strength and binding properties in concrete. The abundance of oxygen in the EDS analysis is consistent with the oxygen atoms present in the chemical structure of cement compounds. In addition, other elements present in cement include aluminum (Al), magnesium (Mg), potassium (K), and iron (Fe) with relatively lower weight

percentages. These elements may originate from the raw materials used in cement production or from minor impurities present in the cement composition.

The EDS analysis of silica fume indicates that silica fume predominantly consists of silicon (Si) and oxygen (O) (Fig. 10b). This composition aligns with the known characteristics of silica fume, which is a highly reactive amorphous material primarily composed of finely divided silicon dioxide (SiO_2) particles. The high silicon content observed in the EDS analysis confirms the presence of amorphous silica in the silica fume sample. The abundance of oxygen in the EDS analysis is consistent with the oxygen atoms present in the silica fume structure. Oxygen is an essential component of silica dioxide (SiO_2) molecules, forming strong bonds with silicon atoms. The absence or low concentrations of other elements, such as aluminum (Al), calcium (Ca), and iron (Fe), confirm the purity and consistency of the silica fume sample.

In the case of polypropylene fiber, a type of thermoplastic polymer composed of carbon and hydrogen atoms, it is known to have high carbon content and low hydrogen content. Therefore, in the EDS analysis of PP fiber, the predominant observation is the presence of carbon (C) peaks (Fig. 10c). The absence of significant peaks for other elements like oxygen (O), silicon (Si), calcium (Ca), and others confirms the predominantly carbon-based composition of the fiber.

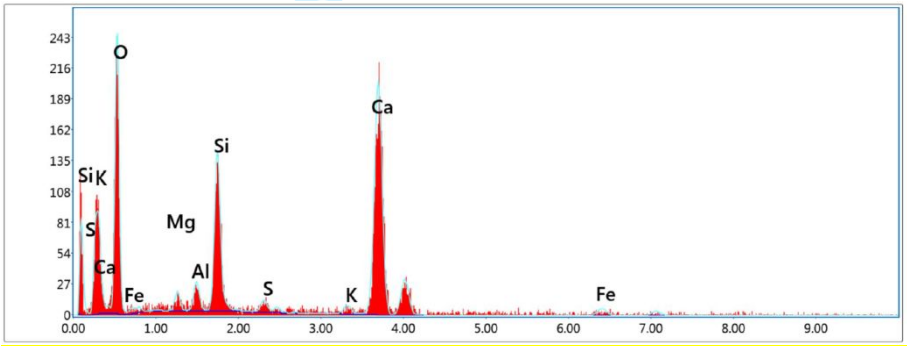

(a)

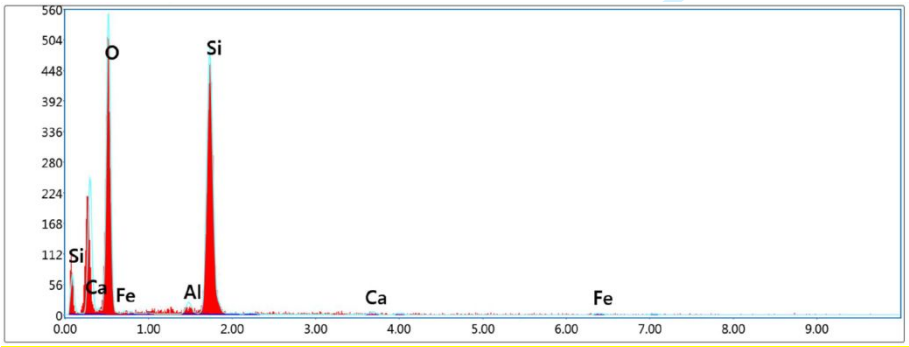

(b)

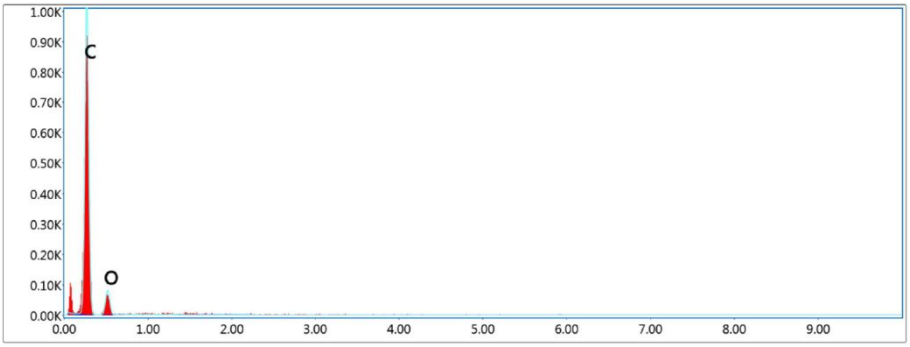

(c)

Fig. 10 EDS analysis of raw materials: (a) Portland cement, (b) Silica fume, and (c) Polypropylene fiber

3.3.2. Printed mortar

This section focuses on the analysis of the microstructure of the printed specimens. The specimens were printed using the determined initial printable time and subsequently crushed into smaller pieces for examination under a Scanning Electron Microscope (SEM). Microscopic images and the results of Energy-Dispersive X-ray Spectroscopy (EDS) analysis were obtained and are presented in Fig. 11a-b, Fig. 12-13, respectively.

Upon careful observation, the microstructure of the printed plain mortar exhibited various phase components, including cement gel (calcium silicate hydrate), calcium hydroxide, and air voids (Fig. 11a). On the other hand, in the case of fiber reinforced mortar, the microstructure revealed the presence of microfibers (Fig. 11b-d). As the volume fraction of fibers increased, a greater number of fibers became visible in the microstructure. It is noting that a significant amount of air voids was observed in the printed cement mortar. This can be attributed to the extrusion process and limited compaction during printing, leading to the entrapment of air within the mortar structure.

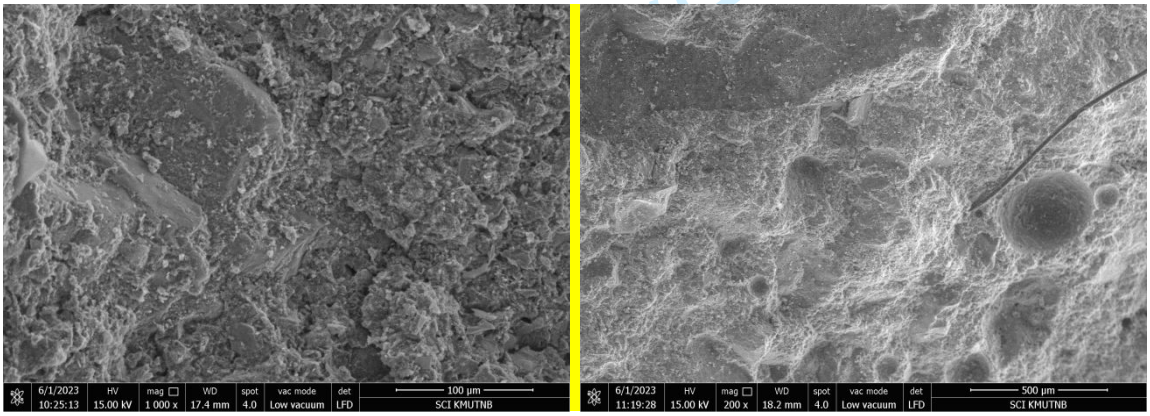

(a) (b)

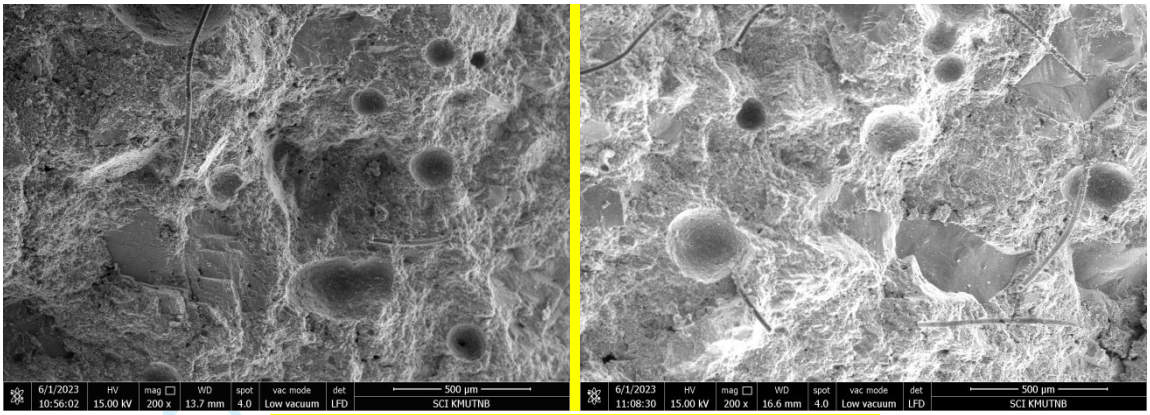

(c) (d)

Fig. 11 SEM images of printed samples a) M0, b) MF25, c) MF50 and d) MF100

The EDS analysis of plain mortar (M0) from all 3 spots demonstrates major elements such as calcium (Ca), silicon (Si), aluminium (Al), and oxygen (O), which are characteristic elements of cementitious materials (Fig.12). In cement-based materials, Portland cement is commonly used as the primary component, and it contains significant amounts of calcium silicates ($CaSiO_3$ and Ca_3SiO_5) as the main constituents. Additionally, the sand used as an aggregate in the mortar mix also contains silicon dioxide (SiO_2), which further contributes to the silicon detected in the analysis. This explains the prominent presence of calcium and silicon in the EDS analysis results. As the cement undergoes hydration reactions with water (H_2O) during the curing process, it leads to the formation of calcium hydroxide ($Ca(OH)_2$) and calcium-silicate-hydrate (C-S-H) gel. These hydration products contribute significantly to the observed oxygen content in the EDS analysis.

In the case of fiber reinforced mortar, the MF100 sample was selected as a representative of this group (Fig. 13). EDS analysis was performed at three different spots: Spot-1, located at the fiber, and Spot-2 and Spot-3, located within the mortar matrix. The results obtained from Spot-2 and Spot-3 showed similarities to those observed in M0 mortar, with significant amounts of calcium, silicon, aluminum, and oxygen detected. However, at the fiber location (Spot-1), a notable spike in the carbon phase (C) was observed. This can be attributed to the microstructure of the polypropylene fibers, which are composed of long chains of carbon and hydrogen. This finding aligns with the previous EDS analysis results of the polypropylene fibers discussed earlier, further confirming the presence of carbon in the fiber-reinforced mortar microstructure.

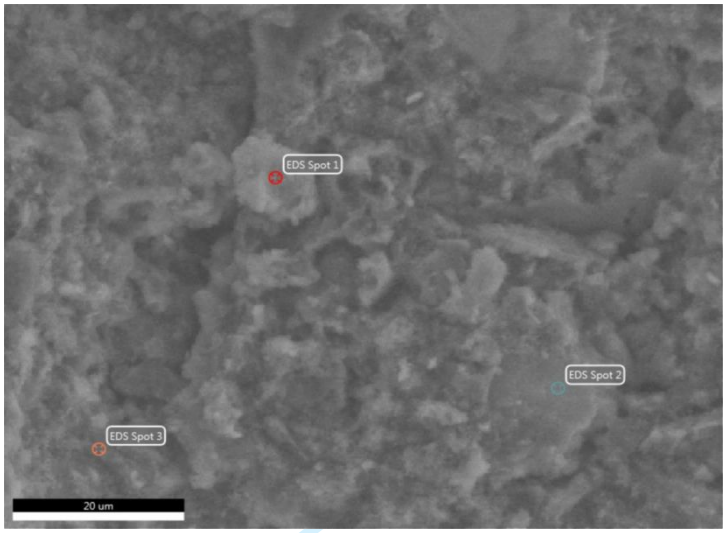

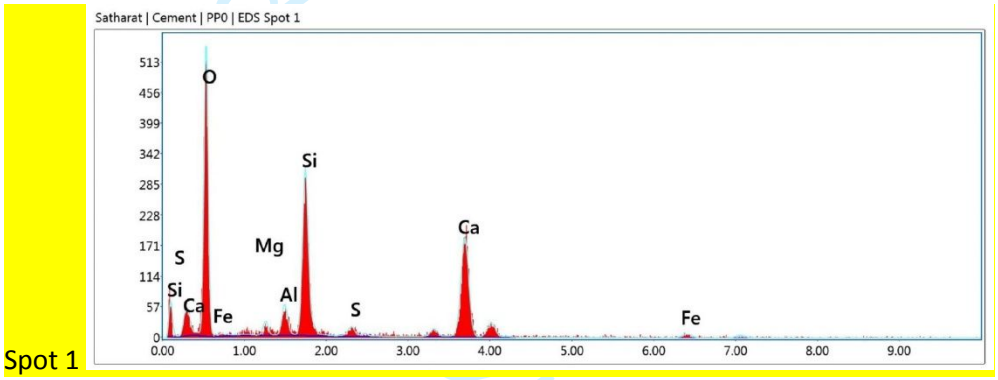

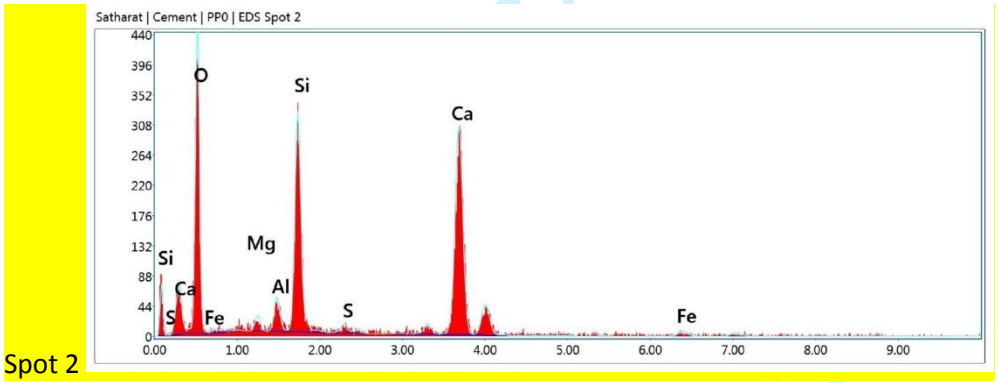

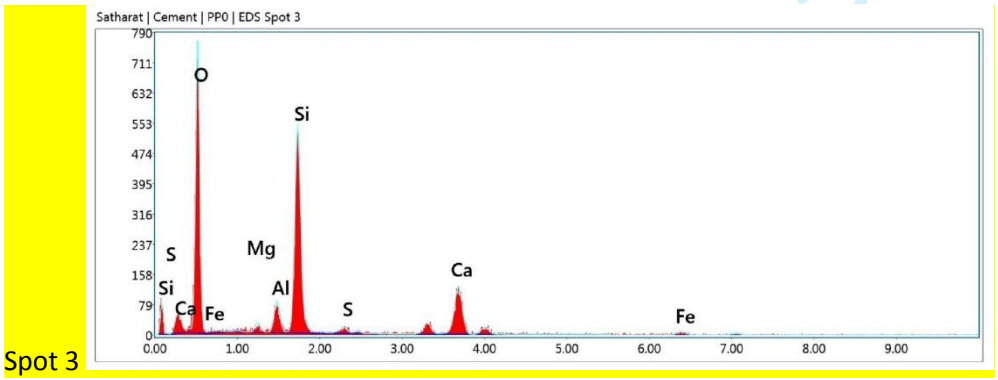

Fig. 12 EDS analysis of printed plain mortar (M0)

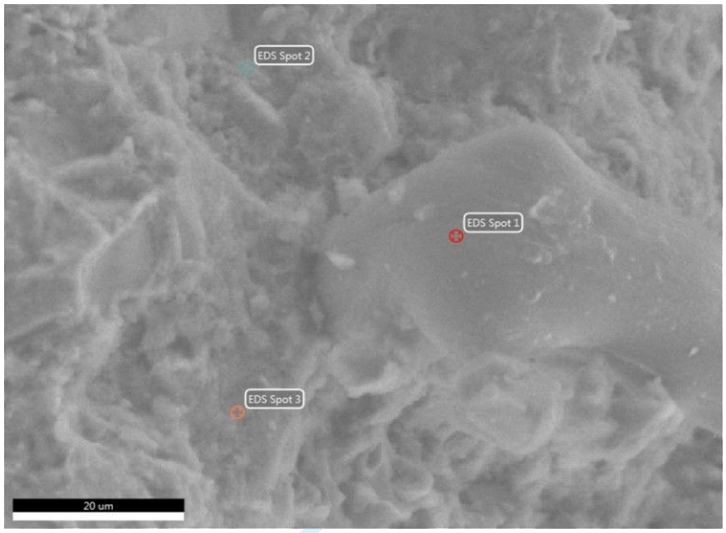

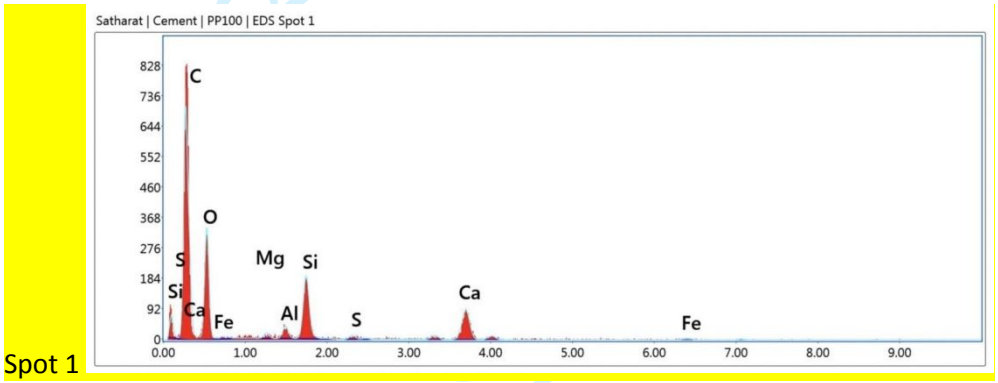

Spot 1

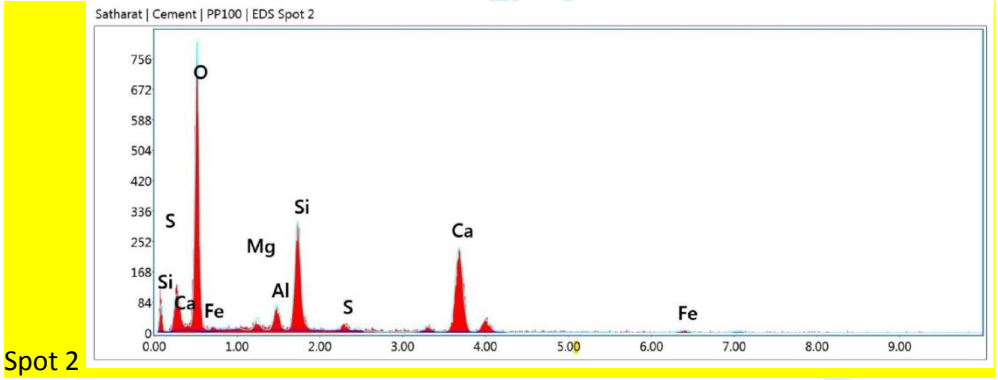

Spot 2

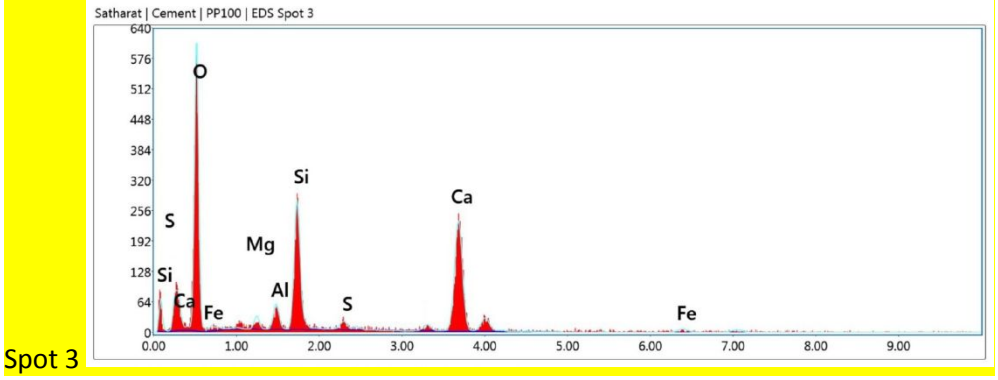

Spot 3

Fig. 13 EDS analysis of printed fiber reinforced mortar (MF100)

4. Conclusion

Based on the obtained results, the following conclusions can be drawn:

- This study successfully introduces a new technique to determine the initial printable time of printed mortar filaments with improved precision, using the relationships between dimension change and time and a simple mathematical procedure.
- The results demonstrate that fiber-reinforced mortar (FRM) exhibits smaller initial printable times compared to plain mortar, with the initial printable time decreasing from 72.5 to 58.5 minutes as the fiber content increases from 0 to 0.1% by volume.
- The calculated initial expected width and height of the printed filament using the obtained initial printable time align closely with the actual measurements, confirming the accuracy of the proposed technique in determining the initial printable time.
- The presence of micro-polypropylene fibers (MF) in the mortar leads to narrower and taller filaments compared to plain mortar (M0). The fibers provide support to the fresh mortar, helping maintain the shape of the printed filament and resulting in reduced layer deformations and strains in MF.
- In term of layer strain, it was found to decrease with the increasing fiber content. The highest layer strain was observed in M0 at 0.16, 0.22, 0.26, and 0.27 for ε_2, ε_3, ε_4, and ε_5, respectively. The lowest layer strain was observed in MF100 at 0.07, 0.10, 0.13, and 0.17 for ε_2, ε_3, ε_4, and ε_5, respectively.
- Suggested future studies include:
    - Long-term durability studies on printed mortar structures to assess the effects of fiber reinforcement on the resistance to cracking, deformation, and degradation over time.
    - Investigate the scalability of the proposed technique by conducting experiments on larger-scale 3D printers or industrial printing systems.
    - Explore the potential of integrating sensors or monitoring systems into the printed structures to continuously monitor the performance and behavior of the mortar during and after the printing process.

5. Acknowledgements

This research is funded by the National Research Council of Thailand (NRCT), and the National Science, Research and Innovation Fund (NSRF) and King Mongkut's University of Technology North Bangkok (KMUTNB) under the contract no. KMUTNB-FF-66-02.

References

[1] Kenton, W. (2020), Labour Intensive, 2020, Retrieved from: https://www.investopedia.com/terms/l/laborintensive.asp#:~:text=Advances%20in%20technology%20and%20worker,to%20be%20more%20labor%2Dintensive

[2] Chantanusornsiri, W. (April, 2021), An ageing conundrum, Retrieved from: https://www.bangkokpost.com/business/2100451/an-ageing-conundrum

[3] The World Bank (June, 2021), Aging and the Labor Market in Thailand, Retrieved from : https://www.worldbank.org/en/country/thailand/publication/aging-and-the-labor-market-in-thailand

[4] McKensey & Company (2019), The impact and opportunities of automation in construction, Retrieved from: https://www.mckinsey.com/business-functions/operations/our-insights/the-impact-and-opportunities-of-automation-in-construction

[5] Buswell, R.A., Leal de Silvab, W.R., Jonesc, S.W., Dirrenbergerd J. (2018). 3D printing using concrete extrusion: A roadmap for research. Cement and Concrete Research, 112: 37-49. https://doi.org/10.1016/j.cemconres.2018.05.006

[6] Le, T.T., Austin, S., Lim, S., Buswell, R.A., Gibb, A.G.F., Thorpe, T. (2012). Mix design and fresh properties for high-performance printing concrete. Materials and Structures, 45, 1221–1232. https://doi.org/10.1617/s11527-012-9828-z

[7] Le, T.; Austin, S., Lim, S.; Buswell, R.A., Law, R., Gibb, A., Thorpe, T. (2012). Hardened properties of high-performance, printing concrete. Cement and Concrete Research, 42, 558–566. https://doi.org/10.1016/j.cemconres.2011.12.003

[8] Ma, G., Li, Z. and Wang, L. (2018). Printable properties of cementitious material containing copper tailings, Construction and Building Materials, 162, 613–627. https://doi.org/10.1016/j.conbuildmat.2017.12.051

[9] Sukontasukkul, P., Panklum, K., Maho, B., Banthia, N., Jongvivatsakul, P., Imjai, T., Sata, V., Limkatanyu, S., Chindaprasirt, P. (2022). Effect of synthetic microfiber and viscosity modifier agent on layer deformation, viscosity, and open time of cement mortar for 3D printing application. Construction and Building Materials, 319, 126111. https://doi.org/10.1016/j.conbuildmat.2021.126111

[10] Chen, Y., Figueiredo, S.C., Li, Z., Chang, K.J.Z.,Çopuroğlu, O.,Schlangen, E. (2020), Improving printability of limestone-calcined clay-based cementitious materials by using viscosity-modifying admixture, Cement and Concrete Research, 132, 106040. https://doi.org/10.1016/j.cemconres.2020.106040

[11] Y. Zhang, Y.S. Zhang, W, She, L. Yang, G.J. Liu, Y.G. Yang, Rheological and harden properties of the high-thixotropy 3D printing concrete. Construction and Building Materials, 201, 278-285. https://doi.org/10.1016/j.conbuildmat.2018.12.061

[12] Y. Zhang, Y.S. Zhang, G.J. Liu, Y.G. Yang, M. Wu, B. Pang, (2018). Fresh properties of a novel 3D printing concrete ink. Construction and Building Materials, 174, 263-271. https://doi.org/10.1016/j.conbuildmat.2018.04.115

[13] Rubio, M., Sonebi, M., & Amziane, S. (2017). 3D printing of fibre cement-based materials: fresh and rheological performances. Academic Journal of Civil Engineering, 35(2), 480-488. https://doi.org/10.26168/icbbm2017.74

[14] Y.W. Wu, C. Liu, H.W. Liu, Z. Zhang, C.H. He, S.H. Liu, R.F. Zhang, Y.Q. Wang, G.L. Bai (2021). Study on the rheology and buildability of 3D printed concrete with recycled coarse aggregates. Journal of Building Engineering, 42, 103030. https://doi.org/10.1016/j.jobe.2021.103030

[15] Lim, S., Buswell, R.A., Le, T., Austin, S., Gibb, A., Thorpe, T. (2012). Developments in construction-scale additive manufacturing processes. Automation in Construction, 21, 262–268. https://doi.org/10.1016/j.autcon.2011.06.010

[16] Ma, G., Wang, L., Ju, Y. (2017). State-of-the-art of 3D printing technology of cementitious material—An emerging technique for construction. Science China Technological Science, 61, 475–495. https://doi.org/10.1007/s11431-016-9077-7

[17] Ashrafi, N., Duarte, J.P., Nazarian, S., Meisel, N.A. (2018). Evaluating the relationship between deposition and layer quality in large-scale additive manufacturing of concrete. Virtual Phys. Prototyping, 14, 135–140. https://doi.org/10.1080/17452759.2018.1532800

[18] Chen, Y., Rodriguez, C.R., Li, Z., Chen, B., Çopuroğlu, O., Schlangen, E.(2020).Effect of different grade levels of calcined clays on fresh and hardened properties of ternary-blended cementitious materials for 3D printing, Cement and Concrete Composites.114, 103708. https://doi.org/10.1016/j.cemconcomp.2020.103708

[19] Wongprachum, W., Sappakittipakorn, M., Sukontasukkul, P., Chindaprasirt, P., Banthia,N. (2018). Resistance to sulfate attack and underwater abrasion of fiber reinforced cement mortar,

Construction and Building Materials, 189, 686-694, https://doi.org/10.1016/j.conbuildmat.2018.09.043

[20] Fu, Q., Xu, W., Bu, M,Guo, B., Niu, D.(2021). Orthogonal experimental study on hybrid-fiber high-durability concrete for marine environment, Journal of Materials Research and Technology, 13, 1790-1804. https://doi.org/10.1016/j.jmrt.2021.05.088

[21] Maho, B., Jamnam, S., Sukontasukkul, P., Fujikake, K., Banthia, N. (2017). Preliminary Study on Multilayer Bulletproof Concrete Panel: Impact Energy Absorption and Failure Pattern of Fibre Reinforced Concrete, Para-Rubber and Styrofoam Sheets, Procedia Engineering, 210, 369-376, https://doi.org/10.1016/j.proeng.2017.11.090

[22] Sukontasukkul, P., Jamnam, S., Rodsin, K., Banthia, N., (2013). Use of rubberized concrete as a cushion layer in bulletproof fiber reinforced concrete panels. Construction and Building Materials. 41, 801-811. https://doi.org/10.1016/j.conbuildmat.2012.12.068

[23] Sukontasukkul, P., Mindess, S. (2003). The shear fracture of concrete under impact loading using end confined beams. Materials and Structures. 36, 372–378. https://doi.org/10.1007/BF02481062

[24] Guo, H., Jiang, L., Tao, J., Chen, Y., Zheng, Z., Jia, B.(2021). Influence of a hybrid combination of steel and polypropylene fibers on concrete toughness. Construction and Building Materials. 275,122132. https://doi.org/10.1016/j.conbuildmat.2020.122132

[25] Sukontasukkul, P. (2004). Tensile behaviour of hybrid fibre-reinforced concrete. Advances in Cement Research. 16(3), 115-122. https://doi.org/10.1680/adcr.2004.16.3.115

[26] Sukontasukkul, P., Sutthiphasilp, T., Chalodhorn, W., Chindaprasirt, P. (2019). Improving Thermal Properties of Exterior Plastering Mortars with Phase Change Materials with Different Melting Temperatures: Paraffin and Polyethylene Glycol, Advances in Building Energy Research. 13(2). https://doi.org/10.1080/17512549.2018.1488614

[27] Sukontasukkul, P., Nontiyutsirikul, N., Songpiriyakij, S., Sakai, K., and Chindaprasirt, P. (2016). Use of Phase Change Material to Improve Thermal Properties of Lightweight Geopolymer Panel, Materials and Structures, 49(11), 4637–4645. https://doi.org/10.1617/s11527-016-0812-x

[28] Sukontasukkul, P., Intawong, E., Preemanoch, P., Chindaprasirt, P. (2016). Use of paraffin impregnated lightweight aggregates to improve thermal properties of concrete panels, Materials and Structures. 49(5), 1793–1803. https://doi.org/10.1617/s11527-015-0612-8

[29] Sukontasukkul, P., Uthaichotirat, P., Sangpet, T., Sisomphon, K., Newlands, M., Siripanichgorn, A., Chindaprasirt, P. (2019). Thermal properties of lightweight concrete incorporating high contents of phase change materials, Construction and Building Materials, 207, 431-439. https://doi.org/10.1016/j.conbuildmat.2019.02.152

[30] Sukontasukkul, P., Sangpet, T., Newlands, M., Tangchirapat, W., Limkatanyu, S., Chindaprasirt, P. (2020). Thermal behaviour of concrete sandwich panels incorporating phase change material, Advances in Building Energy Research, 16(1), 64-88. https://doi.org/10.1080/17512549.2020.1788990

[31] Uthaichotirat, P. Sukontasukkul, P., Jitsangiam, P., Suksiripattanapong, C., Sata, V., Chindaprasirt, P. (2020). Thermal and sound properties of concrete mixed with high porous aggregates from manufacturing waste impregnated with phase change material, Journal of Building Engineering, 29, 101111. https://doi.org/10.1016/j.jobe.2019.101111

[32] Sukontasukkul, P., Sangpet, T., Newlands, M., Yoo, D.Y., Tangchirapat, W., Limkatanyu, S., Chindaprasirt, P. (2020). Thermal storage properties of lightweight concrete incorporating phase change materials with different fusion points in hybrid form for high temperature applications, Heliyon, 6(9), e04863. https://doi.org/10.1016/j.heliyon.2020.e04863

[33] Malaeb, Z., Hachem, H., Tourbah, A., Maalouf, T., Zarwi, N.E., Hamzeh, F. (2015). 3D Concrete Printing: Machine and Mix Design. International Journal of Civil Engineering Technology,6, 14–22.

[34] Khalil, N., Aouad, G., El Cheikh, K., Rémond, S. (2017). Use of calcium sulfoaluminate cements for setting control of 3D-printing mortars. Construction and Building Materials, 157, 382–391. https://doi.org/10.1016/j.conbuildmat.2017.09.109

[35] Ma, G., Li, Z., Wang, L. (2018). Printable properties of cementitious material containing copper tailings for extrusion based 3D printing. Construction and Building Materials, 162, 613-627. https://doi.org/10.1016/j.conbuildmat.2017.12.051

[36] Chen, Y., He, S., Gan, Y., Çopuroğlu, O., Veer, F., Schlangen, E. (2022). A review of printing strategies, sustainable cementitious materials and characterization methods in the context of extrusion-based 3D concrete printing, Journal of Building Engineering. 45, 103599. https://doi.org/10.1016/j.jobe.2021.103599

[37] Li, Z., Wang, L., Ma, G. (2018). Method for the Enhancement of Buildability and Bending Resistance of 3D Printable Tailing Mortar, International Journal of Concrete Structures and Materials.12, 37. https://doi.org/10.1186/s40069-018-0269-0

[38] Chen, M., Yang, L., Zheng, Y., Li, L., Wang, S., Huang, Y., Zhao, P., Lu, L., Cheng, X. (2021). Rheological behaviors and structure build-up of 3D printed polypropylene and polyvinyl alcohol fiber-reinforced calcium sulphoaluminate cement composites, Journal of Materials Research and Technology, 10, 1402-1414. https://doi.org/10.1016/j.jmrt.2020.12.115

[39] Ma, G., Li, Z., Wang, L., Wang, F., Sanjayan, J. (2019). Mechanical anisotropy of aligned fiber reinforced composite for extrusion-based 3D printing, Construction and Building Materials, 202, 770-783. https://doi.org/10.1016/j.conbuildmat.2019.01.008

[40] Sun, X., Zhou, J., Wang, Q., Shi, J., Wang, H. (2021). PVA fibre reinforced high-strength cementitious composite for 3D printing: Mechanical properties and durability. Additive Manufacturing, 102500. https://doi.org/10.1016/j.addma.2021.102500

[41] Zhang, H., Zhu, L., Zhang, F., Yang, M. (2021). Effect of Fiber Content and Alignment on the Mechanical Properties of 3D Printing Cementitious Composites, Materials, 14(9), 2223. https://doi.org/10.3390/ma14092223